PAGEOPH, Vol. 143, No. 1/2/3 (1994) 0033-4553/94/030181-21$1.50 + 0.20/0

Petrophysical Study of Faults in Sandstone Using Petrographic Image Analysis and X-ray Computerized Tomography

M. ANTONELLINI,[1] A. AYDIN,[1] D. D. POLLARD[1] and P. D'ONFRO[2]

Abstract—Petrographic image analysis (PIA) and X-ray computerized tomography (CT) provide local determinations of porosity in sandstone. We have investigated small faults called deformation bands in porous sandstones using these techniques. Because the petrophysical properties of the fault rock vary at a small scale (mm scale), the ability of PIA and CT to determine porosity in small volumes of rock and to map porosity distribution in two and three dimensions is crucial. This information is used to recognize the processes involved in fault development and the different kinds of microstructures associated with dilatancy and compaction. The petrophysical study of fault rock in sandstone permits one to make predictions of the hydraulic properties of a fault and thereby evaluate the sealing or fluid transmitting characteristics of faulted reservoirs and aquifers. The results of this study indicate that faulting in sandstone alters the original porosity and permeability of the host rock: the porosity is reduced by an order of magnitude and the permeability is reduced by one to more than seven orders of magnitude for faults associated with compaction.

Key words: Cataclasis, fluid flow, fault, video image analysis, X-ray computerized tomography, porosity, permeability.

Introduction

In this paper we present two methods of characterizing the petrophysical properties (e.g., porosity, permeability, capillary pressure) of faults in sandstone. These methods are Petrographic Image Analysis (PIA) (EHRLICH *et al.*, 1991; ANTONELLINI *et al.*, 1994) and X-ray Computerized Tomography (CT) (WELLINGTON and VINEGAR, 1987; VINEGAR *et al.*, 1991). This study is primarily concerned with the measurement of porosity. We present examples of applications of these methods to the porosity determination of small faults in sandstone and summarize the results of a broader project aimed at understanding microstructure and fluid flow properties of faults (ANTONELLINI *et al.*, 1994; ANTONELLINI and AYDIN, 1994; ANTONELLINI and AYDIN, in preparation). Here we also present new data obtained with CT and compare these with those obtianed by PIA. We demonstrate

[1] Department of Geological and Environmental Sciences, Stanford University, Stanford, CA 94305-2115, U.S.A.

[2] Conoco Inc., P.O. Box 1257, Ponca City, OK 74603, U.S.A.

the integration of all petrophysical property measurements for formulating a model for fluid flow in fault zones in sandstone.

The concept of weak faults and the associated state of stress (ZOBACK *et al.*, 1987) has renewed considerable interest in the fluid pressure distribution in crustal scale faults (e.g., BYERLEE, 1990, 1993; RICE, 1992). Important parameters influencing the fluid pressure distribution in and around fault zones are the volumetric component of the deformation and the hydraulic properties of fault zones. In fact, dilatation and/or compaction associated with faulting (SLEEP and BLANPIED, 1992), and the permeability along and across fault zones (RICE, 1992; BYERLEE, 1993) are critical elements in recent fault models concerned with the instability responsible for earthquakes.

The permeability and sealing capacity of faults have also attracted interest for practical reasons. Ground water levels often change across faults (ROBISON *et al.*, 1988; MACLAY and LAND, 1988), and overpressurized fault zones pose serious problems for underground construction (HENDERSON, 1939). Furthermore, sealing faults compartmentalize oil and gas reservoirs and constitute hydrocarbon traps (DOWNEY, 1984; HARDMAAN and BOOTH, 1991; KNOTT, 1993). For example, in the North Sea, the majority of faults are sealing for hydrocarbons, presenting serious problems for exploration, drilling, and production.

The petrophysical properties of deformed rocks provide information regarding physical processes that take place during faulting. In addition, the petrophysical properties reveal how the faults may affect the fluid flow in a porous sandstone. Small-offset faults in sandstone are called deformation bands (AYDIN, 1978; AYDIN and JOHNSON, 1983; ANTONELLINI *et al.*, 1994); deformation bands are quasi-tabular structures, about 1 mm thick, that accommodate offsets on the order of 1–30 mm (Fig. 1a). Deformation bands tend to localize in "zones of deformation bands" accommodating offsets on the order of 0.1–0.5 m; offset of a meter or more is usually associated with the development of a slip plane (Fig. 1b) that represents a discontinuity in the rock mass.

The formation of deformation bands has been associated with grain crushing and porosity reduction (AYDIN, 1978; UNDERHILL and WOODCOCK, 1987), but ANTONELLINI *et al.* (1994) have documented that this is not always the case. The microstructure of deformation bands is strongly dependent on the porosity, the sorting of grains, the clay content of the host rock and the mean stress, $(\sigma_1 + \sigma_2 + \sigma_3)/3$, at the time of deformation. The microstructures control petrophysical properties of faults and fault zones such as porosity, permeability and capillary pressure (PITTMAN, 1981; NELSON, 1985). Where grain crushing and porosity reduction are the dominant mechanisms of deformation, large capillary pressures and low permeabilities give a sealing potential to faults in sandstone. On the other hand, where positive dilatancy accommodates strain during slip, fluid flow may be enhanced.

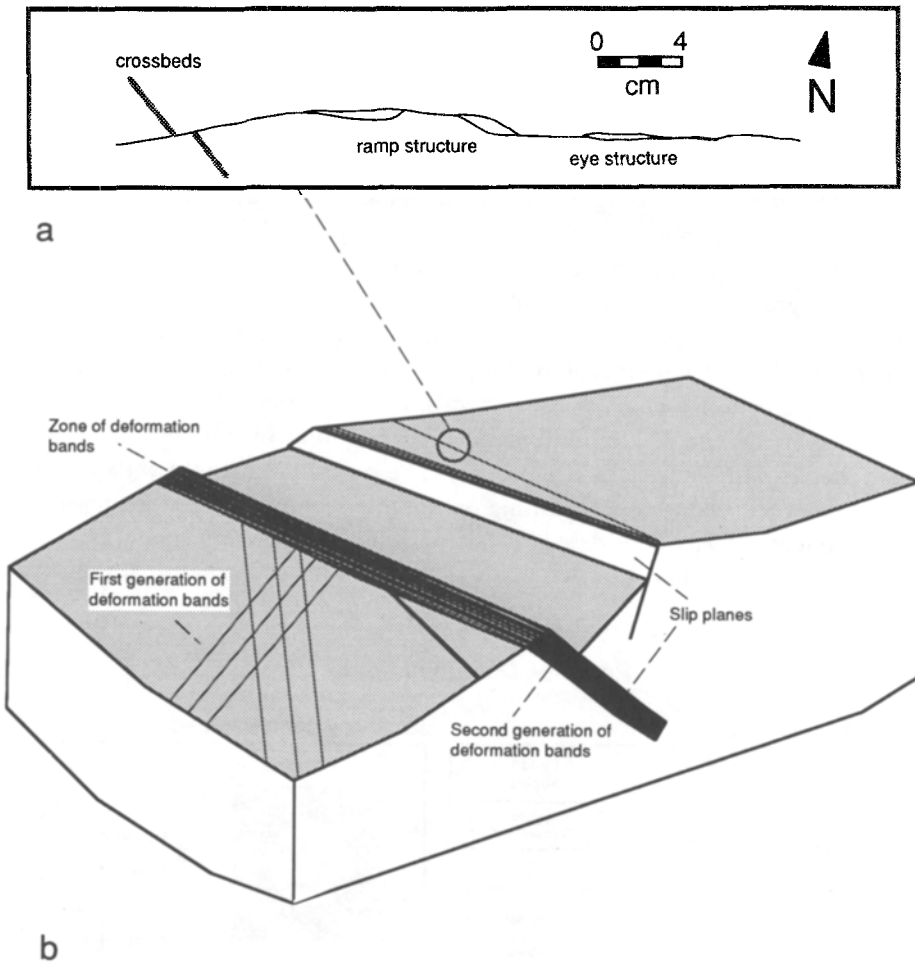

Figure 1
(a) Map of a deformation band in sandstone (Delicate Arch viewpoint, Arches National Park, Utah). The eye and ramp structures are characteristic of the deformation bands. (b) Schematic block diagram representing the evolution of a slip plane from a zone of deformation bands and the two different generations of deformation bands present at Arches National Park.

Methods to Determine Petrophysical Properties in Sandstone

Petrographic Image Analysis

The deformation bands are so thin ($\sim$1 mm) that the standard procedures of porosity determination, based on helium compressibility and made on rock plugs 25 mm in diameter (BOURBIÈ *et al.*, 1987), do not provide an accurate estimate of void volume (and particularly void distribution) within and in the region adjacent

to the band. This lack of accuracy is due to the large volume of the sample, compared to the size of the structure. Therefore, the porosities of the host rock, the deformation band, and the region adjacent to the deformation band (typically a zone 1 mm wide parallel to the band) were measured directly on a thin section impregnated with blue epoxy via a PC-based image analysis system supported by a RTI parallel processor (Recognition Technologies, Inc.) and a video camera (Fig. 2a). The image of a thin section is transmitted from a video camera to an image analysis system where it is processed to separate minerals from pore space using a filter on the gray levels of the pixels.

The process of separation of the minerals from the pore space is called *segmentation*. The filter used (comb filter) can separate the blue of the epoxy filling the pore space from the color of the minerals. Once the image has been segmented, the porosity is determined by automatic pixel counting on selected areas of the image (usually with an area of 0.5–1 mm^2). The porosity measured with the image analyzer was checked by point counting on the thin section. The porosity measured by point counting was considered to be the reference porosity and was used to calibrate the filter so that the two methods produce the same result for the same

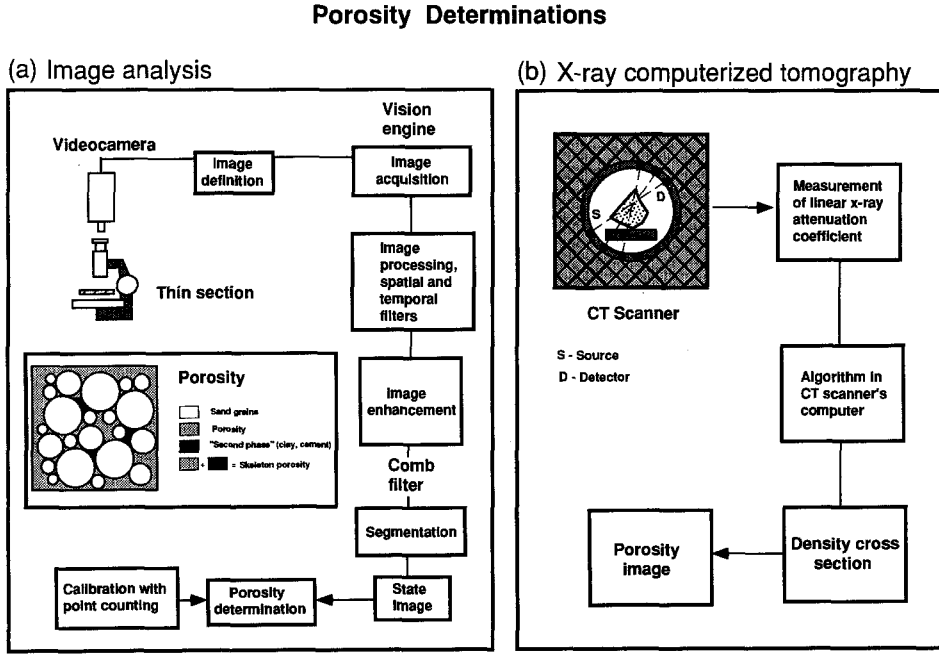

Figure 2

(a) Flow chart illustrating the image processing sequence used to obtain 2D porosity determinations from a thin section using PIA. The inset shows the relationship between sand grains, porosity, secondary phase and skeleton porosity. (b) Flow chart illustrating the processing sequence used to obtain porosity maps of any cross section of a hand-sized rock sample using CT.

image. This operation was performed once on a set of samples with similar lithologic properties. The calibration was then checked at intervals by repeating the point counts. This checking procedure has shown that in clean sandstone the difference between the porosity measurement determined with PIA and that determined by point counting was on the order of 2%. If colored minerals or clays were present in the sample the errors were large and the porosity was determined by physically point counting the video image of the thin section after superposing a rectangular grid on it.

Porosity is defined as the ratio between the volume of voids and the volume of sample. However, in some samples the pore space is filled by "secondary phases" such as authigenic clays, coatings, iron oxides and cement precipitations. Typically these "secondary phases" are the result of weathering and diagenesis and were not present at the time of formation of the deformation bands. In the examples presented here the porosity is equal to the volume of voids plus the volume of the secondary phases divided by the total volume of the sample (Fig. 2a); following BOURBIÈ *et al.* (1987) we call this extended definition of porosity *skeleton porosity*. Where iron oxides, clays and/or grain coatings with dark color made up the secondary phases and completely filled the intergranular space, it was possible to use the filter of the image analyzer to determine the skeleton porosity of the sample. However, if the secondary phases did not fill completely the pore space, or if they were made of cement with the same color as the mineral grains, the skeleton porosity was determined by point counting the video image.

X-ray Computerized Tomography

X-ray computerized tomography is a nondestructive imaging technology developed by HOUNSFIELD (1972) that has become a revolutionary diagnostic tool in medicine. CT combines a series of X-ray radiographs, taken from different angles into an instrument called a CT scanner (Fig. 2b), to obtain a cross-sectional image (i.e., a "slice") via a computer back-projection algorithm (BROOKS and DICHIRO, 1976). Many cross-sectional images can be combined to create a three-dimensional model of the scanned object. CT scanners measure X-ray attenuation and can resolve differences in this quantity on the order of 0.1% within volumes (also called voxels) $\leq 2\,\text{mm}^3$ (WELLINGTON and VINEGAR, 1987). The X-ray attenuation is defined by a quantity μ called the "linear attenuation coefficient" (WELLINGTON and VINEGAR, 1987), which is expressed in the form

$$\mu = \rho(a + bZ^{3.8}/E^{3.2})$$

where ρ is the bulk density, Z the average atomic number (i.e., the average for the chemical composition of the minerals in the rock; e.g., for fused quartz $Z = 11.8$), E the X-ray energy, a the Klein-Nishina coefficient (almost energy independent) and b a constant. Inspection of the above expression reveals that a CT image taken

at high X-ray energy (e.g., 120 kV in our CT) will be particularly sensitive to the bulk density of the sample, whereas a CT image taken at low X-ray energy (e.g., 90 kV in our CT) will be particularly sensitive to the atomic number.

The quantity of interest in our study is the porosity. We know from petrographic analysis that the composition of the two samples analyzed with CT is 97 to 98% quartz and 2–3% feldspars and opaque minerals. By knowing the density (from the high energy CT image) and the composition of the sample it is possible to calculate the porosity at any point (voxel) of the CT image.

The CT scanner used in our experiments is a Delta Scan 100 series and the software used to process the data includes CATPIX (Universal Medical) and the PV Wave programs (Precision Visual Co.). After calibration of the instrument, the error on CT density determination has been calculated (with statistics on dual energy data) to be 1.8% on our samples, whereas the error on atomic number determination has been calculated to be 0.8%.

Applications

Applications of PIA and CT to porosity determinations in deformation bands are presented here to illustrate how these techniques can be used in a petrophysical study of faulted rocks. Figure 3 presents some video images of the microstructure of deformation bands obtained from thin sections. In particular, Figure 3a shows the microstructure of a deformation band in which there has been some increase in volume (positive dilatancy) with respect to the surrounding host rock. This deformation band was sampled in the Moab member of the Entrada Sandstone at Arches National Park (sample sm4). After processing and segmenting the video image one obtains a new image, called the "state" or "binary" image, where the mineral grains are represented in black and the pore space in white (Fig. 4a). On this video image the porosity is determined by selecting an area of 0.5–1 mm^2. It is then possible to make a profile of the porosity variation from the host rock into the deformation band (Fig. 5a). Figures 3 and 4 show other examples of deformation band microstructures and Figure 5a presents a few profiles across deformation bands which show dilatancy, compaction, and/or grain crushing in their microstructure.

CT similarly allows one to make porosity variability profiles starting from a porosity image. Two hand-sized samples containing undeformed sandstone along with deformation bands and/or the wall rock of slip planes have been scanned at an interval of about 10 mm (10 mm-thick slices). These samples did not contain secondary phases in the pore space. Other scans were made at an interval of 2 mm (2 mm-thick slices) by putting a lead collimator on the X-ray source and detectors. The slip plane and most of the deformation bands in the samples were oriented perpendicular to the plane of the scan.

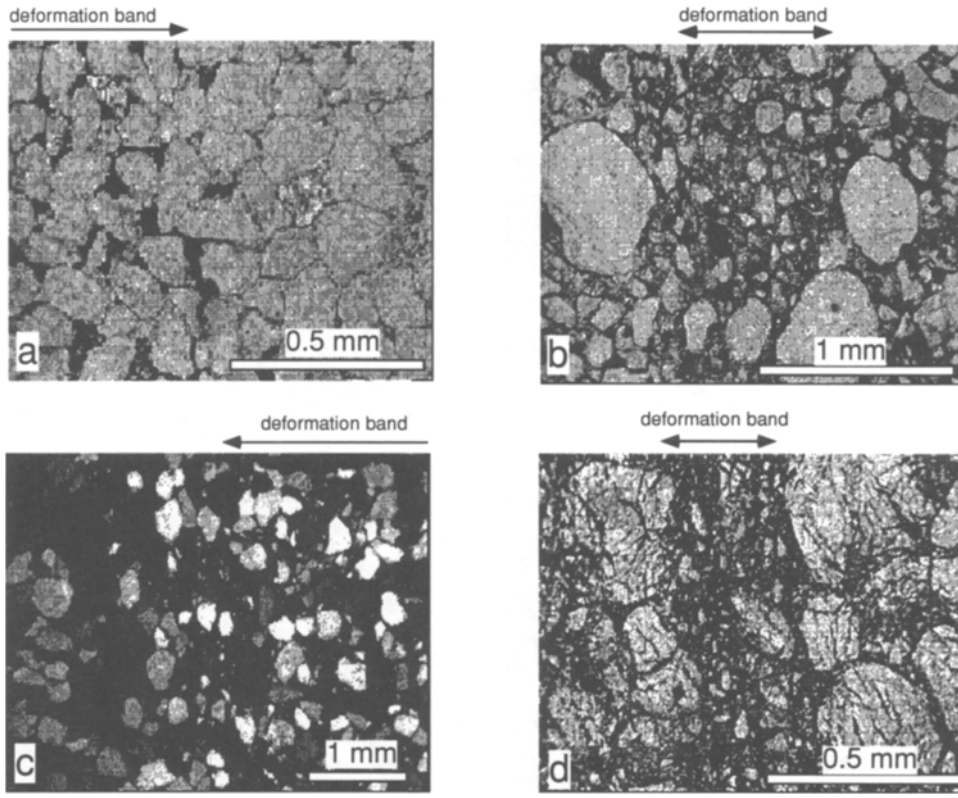

Figure 3
(a) Video image of a dilatant deformation band with no cataclasis in the Moab member of the Entrada Sandstone. (b) Deformation band with no porosity change with respect to the host rock. This deformation band has been observed in a poorly sorted interval of the Slickrock member of the Entrada Sandstone. (c) Deformation band with poorly developed cataclasis in the Moab member of the Entrada Sandstone. (d) Deformation band with well developed cataclasis in the St. Peter Sandstone.

In the experimental configuration that we used, the voxel size, which is the smallest volume over which the density is averaged, is 1 mm × 1 mm × 10 mm for the scans taken every 10 mm, and 1 mm × 1 mm × 2 mm for the scans taken every 2 mm. Porosity images of representative slices (Fig. 6b) have been obtained from the density images (Fig. 6a) in order to map the porosity distribution within the samples and to compare the values with those obtained from image analysis. An example of a porosity profile obtained with CT across a deformation band from the Moab member of the Entrada Sandstone at Arches National Park is given in Figure 7, whereas a porosity profile across a slip plane from the same unit is given in Figure 5b. The porosity in the wall rock of the slip plane is below the limit of measurement for image analysis ($< 1\%$; Fig. 5b), however CT porosity maps (Fig. 6) show that the porosity in the wall rock of the slip plane ranges from 0 to 5%.

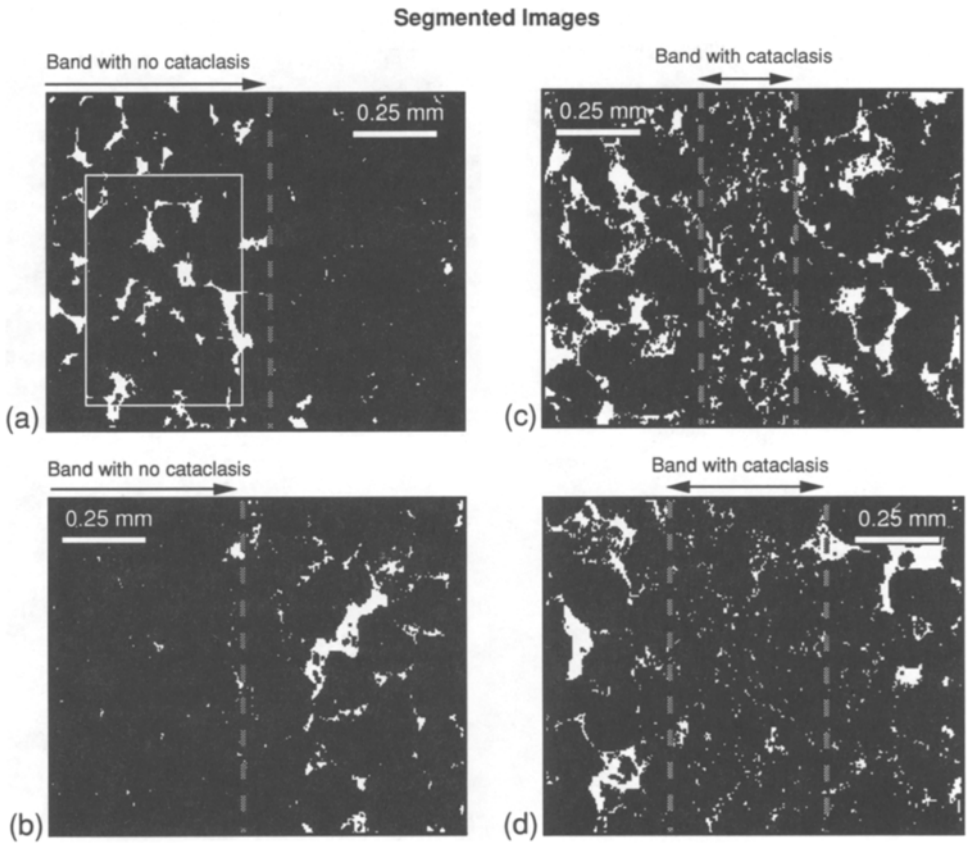

Figure 4

Segmented images of deformation bands from video camera black and white frames. White represents the pore space, black represents the solid phases. (a) Dilatant band with no cataclasis in the Moab member of the Entrada Sandstone; it is the same image shown in Figure 3a (sample sm4). The rectangle represents the sampling volume. (b) Compacted band with no cataclasis in the Moab member of the Entrada Sandstone (sample s24). (c) Deformation band with cataclasis in the Moab member of the Entrada Sandstone. (d) Deformation band with cataclasis at the contact between the Moab and Slickrock members of the Entrada Sandstone (sample s16).

Overview of Characteristics of Faults in Sandstone

The results of the petrophysical study summarized here are part of a broader study on the structural and fluid-flow properties of faults in sandstone. The results of extensive field work, including mapping and sampling, will be presented in ANTONELLINI and AYDIN (in preparation). The reader can find a complete account of the microstructure and micromechanics of deformation bands in ANTONELLINI *et al.* (1994), and of permeability and capillary pressure measurements in ANTONELLINI and AYDIN (1994).

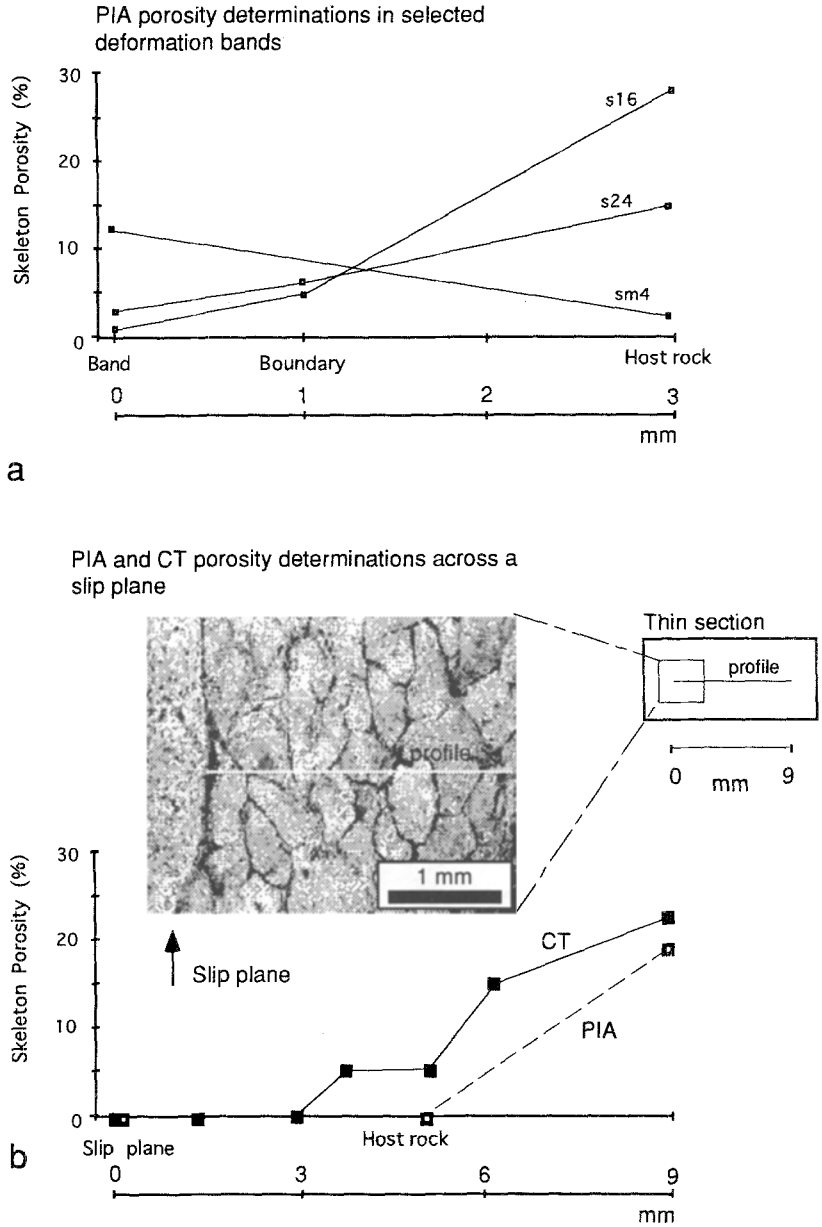

Figure 5

(a) Porosity profiles, obtained with PIA, across deformation bands. Sample s16 contains a deformation band with grain crushing and compaction. Samples s24 and sm4 contain deformation bands with no grain crushing; s24 contains a band with compaction in its microstructure and sm4 contains a band with dilatancy in its microstructure. (b) Porosity profile across the wall rock of a slip plane in the sample of Figure 6. Solid squares are the porosity determinations made with CT, while the empty squares are those made with PIA. A video image showing extensive pressure solution and grain interlocking in the wall rock of the slip plane is shown in the inset. The porosity profile is perpendicular to the slip plane.

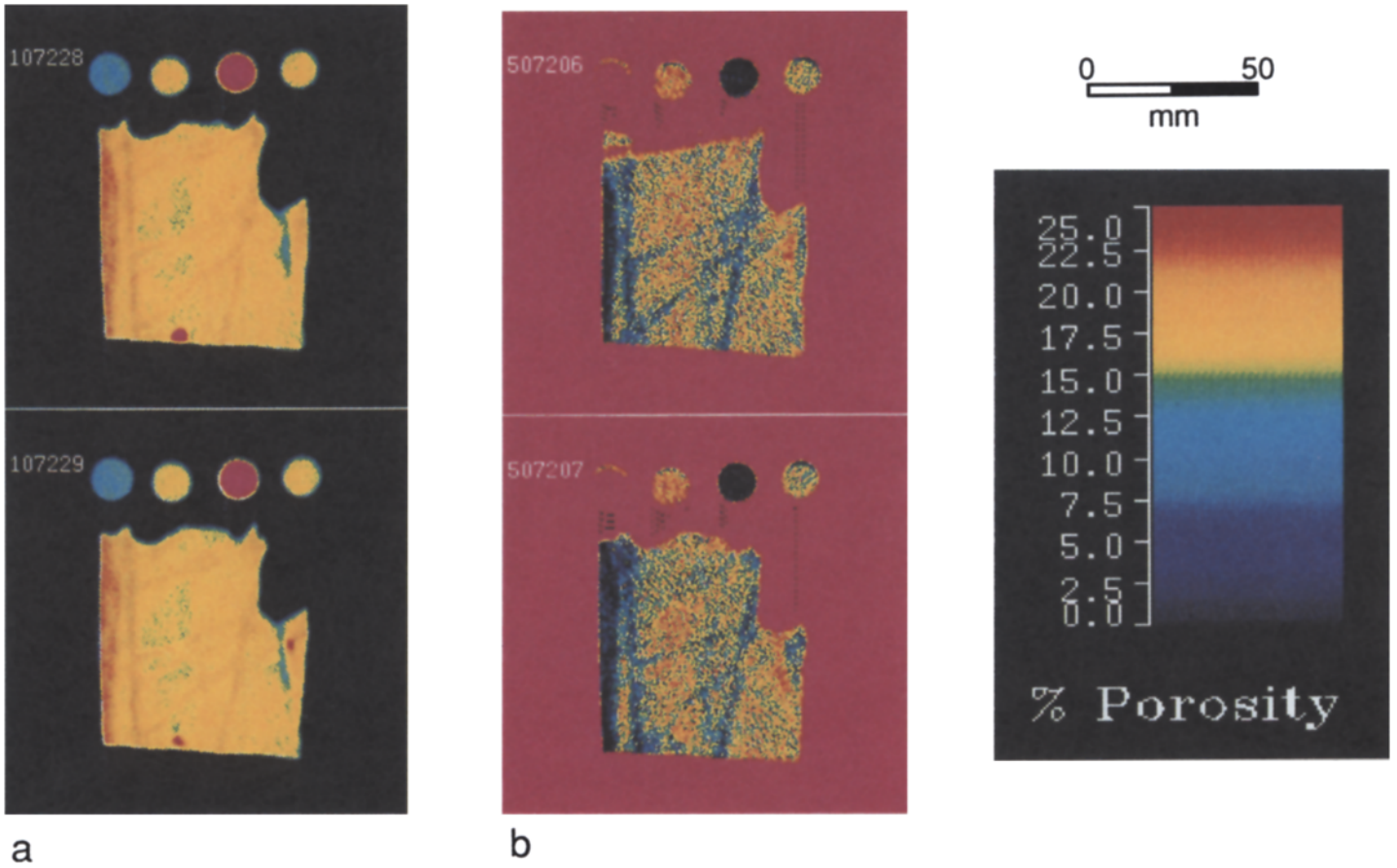

Figure 6

(a) CT image cross section at 120 KV of an Entrada Sandstone sample containing a slip plane (on the left side) and deformation bands. The base of the sample is 57 mm long. The thickness of the slice is 2 mm. The circles are rods of different materials used for density calibration. From left to right: a glass rod filled with Freon 113 (density = 1.565 g/cm^3), a Kel-F polymer rod (density = 2.065 g/cm^3), an aluminum 6061 rod (density = 2.689 g/cm^3), and a fused quartz rod (density = 2.20 g/cm^3). (b) Porosity map obtained from the same cross section but with a slice-thickness of 10 mm. (c) Porosity scale for reference in Figure 6b.

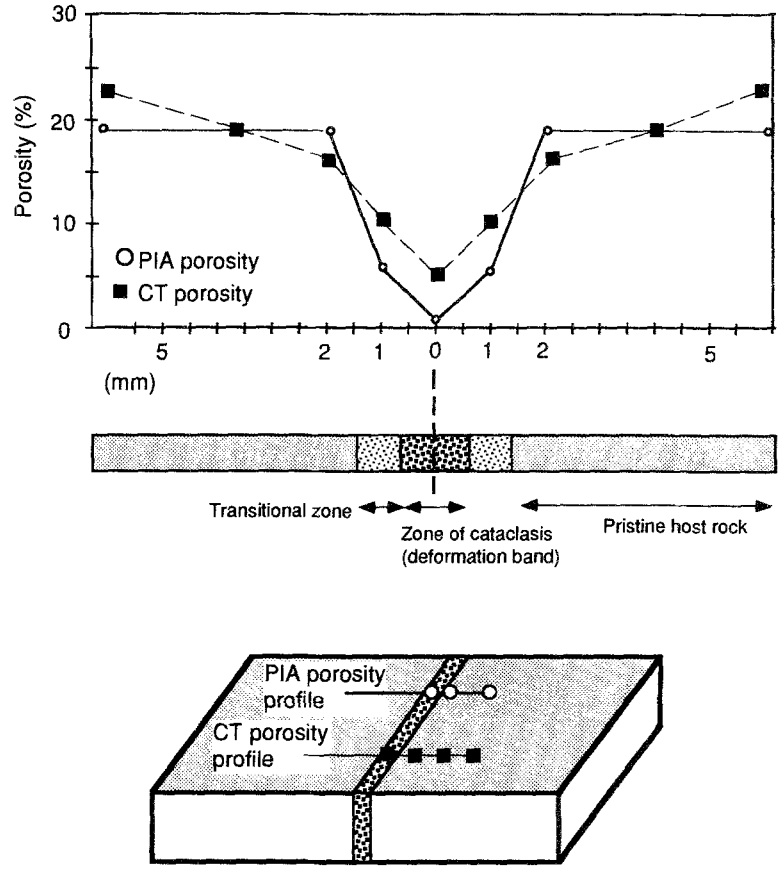

Figure 7

Porosity profile across a deformation band in the Moab member of the Entrada Sandstone. The empty circles represent the data points for porosity determination obtained with image analysis (PIA), whereas the solid squares represent CT porosity for a similar band in the same sample obtained from a porosity map such as the one shown in Figure 6b. The PIA and CT measurements have been made only on the right side of the deformation band shown in the block diagram; the values to the left have been extrapolated to complete the graph.

The microstructures of the samples have been analyzed with standard optical techniques, image analysis, and X-ray computerized tomography (Fig. 2). One hundred thin sections, 85 of which were impregnated with blue epoxy to enable porosity determinations, have been examined. Seventy-eight thin sections are from samples of the Jurassic-Triassic Entrada, Navajo and Wingate Sandstones collected at or near Arches National Park (U.S.A.), the remaining samples come from the Mio-Pliocene Pismo Formation (Central California), the Ordovician St. Peter Sandstone of the Kentland Quarry (Indiana), the Jurassic Aztec Sandstone of the

Valley of Fire (Nevada), and the Eocene Loiano Formation of the Northern Apennines (Italy).

Geometric properties, including band thickness, offset, grain size of the crushed zone and grain size of the host rock, were measured with an optical micrometer. The compositional and textural characteristics were determined by optical microscopy and by point counting. In the following, the reported porosity (skeleton porosity) values were determined via image analysis, and the permeability was measured with a minipermeameter (ANTONELLINI and AYDIN, 1994).

Microstructure and Petrophysical Properties of Faults in Sandstone

Although deformation bands are defined as having common macroscopic characteristics such as small offsets (1–30 mm), systematic interaction patterns (Fig. 1), and lack of a well developed displacement discontinuity plane (ANTONELLINI *et al.*, 1994), they have a broad spectrum of microstructures. By using the techniques described above for making porosity determinations in very small volumes of rock, it was possible to distinguish two kinds of deformation bands on the basis of microstructure and localization characteristics: 1) deformation bands with little or no cataclasis and 2) deformation bands with cataclasis.

Deformation bands with no cataclasis can be identified in thin section by the porosity and/or fabric differences that they display with respect to the host rock (Figs. 3a,b, 4a,b). They appear as an area of increased porosity (Fig. 4a) with respect to the host rock (positive dilatancy), as an area of increased compaction (negative dilatancy; Fig. 4b) or, in the case of no detectable change in volume, as an area with a distinctive fabric defined by the alignment of elongate grains with their axes in the plane of the deformation band (Fig. 3b).

Deformation bands showing positive dilatancy, but very few or no crushed grains, have been observed in sandstones where the porosity of the country rock is less than 12%. For cases where the porosity in the country rock is 4–5%, the porosity in the band can be up to 12–13% (Fig. 9 in ANTONELLINI *et al.*, 1994). The pore filling of these deformation bands often consists of authigenic clays and/or iron oxides precipitated by circulating fluids.

Deformation bands showing compaction, but little or not cataclasis (Fig. 4b) are marked by decreased porosity with respect to the host rock. The porosity in the host rock is usually larger than 18%; within the deformation band the porosity drops to a value that is between one third and two thirds of the host rock porosity (Fig. 9 in ANTONELLINI *et al.*, 1994).

Deformation bands with little or no volume change and no cataclasis usually develop in rocks with very poor sorting (Fig. 3b). The porosity of these bands and their associated host rocks are generally in the range 1–5%.

Deformation bands with cataclasis can be recognized by the presence of grain crushing and porosity reduction. The amount of cataclasis in a deformation band

is variable from a few patches of crushed grains in pods and pockets aligned along a thin line, to a fully developed cataclastic zone about 1 mm thick (Figs. 3c,d, 4c,d). The amount of cataclasis and porosity reduction is greater in bands closer to slip planes (Fig. 6b). Farther away from slip planes the bands tend to have less cataclasis.

Bands with cataclasis vary in thickness from 0.2 to 3 mm regardless of grain size in the host rock. A weak connection exists between thickness of the bands and porosity of the host rock. Thinner bands ($\sim$0.5–0.8 mm) appear to develop preferentially in low-porosity sandstones (porosity $< 15\%$) (Fig. 11 in ANTONELLINI *et al.*, 1994).

The porosity of many deformation bands with cataclasis, determined by image analysis, decreases about one order of magnitude with respect to that of the host rock (Fig. 5). The decrease in porosity within the band appears to be more accentuated where the porosity in the host rock is larger (ANTONELLINI *et al.*, 1994). Feldspar, polycrystalline quartz and rock fragments are the most commonly crushed grains in a deformation band. The feldspars, the polycrystalline quartz and to a certain extent the rock fragments, presumably crush preferentially because of mineral cleavage, grain boundaries, or other preexisting discontinuities.

The permeability perpendicular to deformation bands with cataclasis is affected by the degree of compaction and grain crushing that is present in the microstructure of the faults. Deformation bands with poorly developed cataclasis have a permeability of 10–500 md in host rock where the permeability is 1000–5000 md, whereas in host rocks of the same permeability deformation bands with well-developed cataclasis have a permeability of 0.1–5 md (ANTONELLINI and AYDIN, 1994).

A fault in sandstone, to accommodate increasingly larger amounts of offset, evolves from a single deformation band to a zone of deformation bands, and then into a slip plane (AYDIN and JOHNSON, 1983). The result is the development of a complex fault zone with internal structures that have different petrophysical properties and a very anisotropic permeability (Fig. 8).

The CT and PIA porosity determinations have shown (Figs. 6, 5b) that the material in the wall rock of a slip plane has a very low porosity ($< 1\%$). The porosity and the permeability of deformation bands in sandstone can vary (porosity range 1–29%; permeability range 0.1–600 md in the samples examined here), because the development of these structures involves dilation, compaction and cataclasis, or deformation with no volume change.

The permeability of a large fault zone is affected by the presence of slip planes. The slip planes surfaces can be propped open, thereby providing a greater permeability along the surfaces, whereas a cataclastic zone with compaction in the wall rock of the slip planes reduces the permeability perpendicular to the fault zone (Fig. 8). In the cataclastic zone of deformation bands, this reduction can be as much as four orders of magnitude with respect to that of the undeformed parent rock and more than seven orders of magnitude (from <0.01 md in the wall rock to 10^4 md

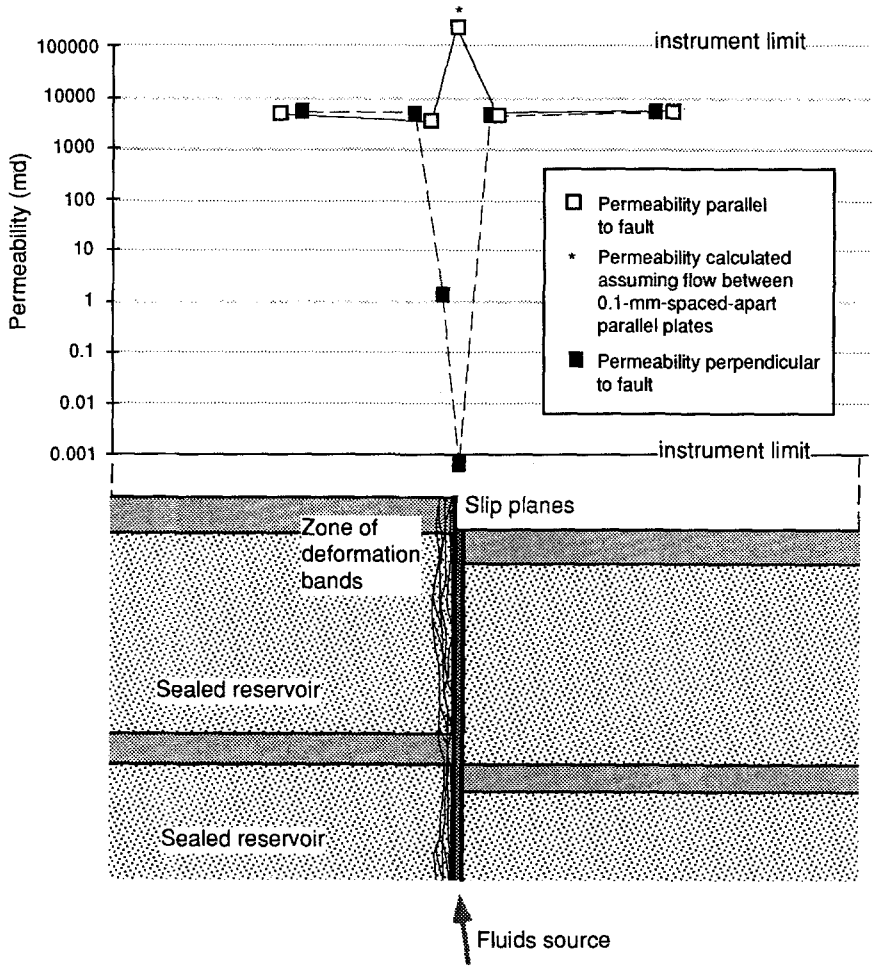

Figure 8

Fluid flow model for a fault in sandstone. Permeability values for the host rock, the zone of deformation bands, and the cataclastic wall rock of the slip plane are from ANTONELLINI and AYDIN (1994). The permeability has been determined with a minipermeameter. The zone of deformation bands and the cataclastic wall rock of the slip plane can seal the reservoirs to the left, whereas slip plane discontinuity can provide a vertical conduit for the fluids.

in the host rock) in the wall rock of the slip surface (ANTONELLINI and AYDIN, 1994). Thus, fault structures in granular rocks may provide an increasing transport capability along the fault, but a sealing response perpendicular to the fault (DOWNEY, 1984; EDWARDS *et al.*, 1993; ANTONELLI and AYDIN, 1994). Even fault zones with a dilatant cataclastic zone may reduce permeability at a later time because the excess volume is usually filled in by precipitates (ANTONELLINI *et al.*, 1994).

Micromechanics of Faults in Sandstone

The porosity determinations obtained with PIA and CT have been critical for developing a micromechanical model for deformation band development (ANTONELLINI *et al.*, 1994). In particular the microstructure of deformation bands can be interpreted in terms of critical state theory (SCHOFIELD and WROTH, 1968; WOOD, 1990), which proposes that a soil or a granular material, when continuously strained, can flow like a fluid with no volume change if it is in a *critical state* (SCHOFIELD and WROTH, 1968). Triaxial experiments on soil samples with different specific volumes (PARRY, 1960) show that some samples deformed by increasing and some by decreasing their volume. The critical state is a function of the mean effective normal stress (p'), the deviatoric stress (q) and the specific volume of the sample (v). In a triaxial experiment (Fig. 9a) a soil sample can deform, after

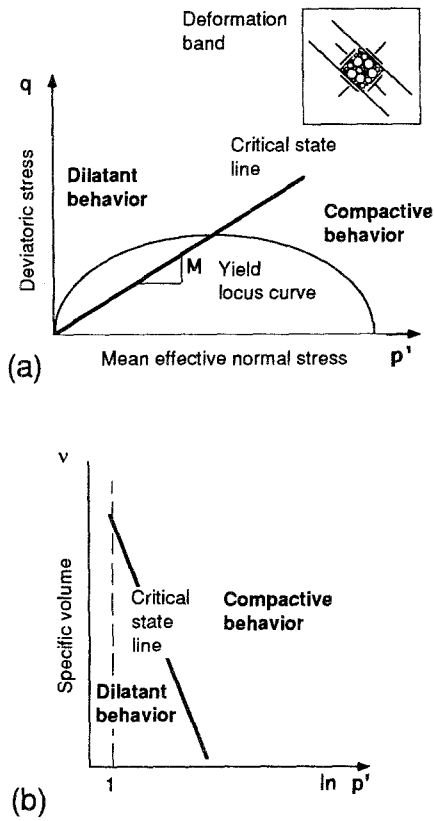

Figure 9

(a) Volumetric strain of a granular aggregate defined as a function of mean effective stress and deviatoric stress. The yield locus for a granular material is shown by the curve. In the field to the left of the critical state line the material dilates after yielding, and in the field to the right it compacts. (b) Volumetric strain of a granular aggregate defined as a function of specific volume and mean effective normal stress. The inset on top right shows the boundary conditions.

yielding (along the elliptical curve), by increasing its volume if q is high and p' is low, or by decreasing its volume if q is low and p' is high. The sample deforms with no volume change at the intersection between the yield locus curve and the line representing the critical state. The slope of this line (M) represents a frictional coefficient.

The critical state also can be defined by considering the specific volume of the sample and the mean effective normal stress during a triaxial experiment (Fig. 9b). In this case the critical state curve is a line on a plot of specific volume versus log of the mean effective normal stress. High deviatoric stress values or low porosity values (low specific volumes) tend to promote positive dilatancy, whereas large values of the mean compressional normal stress and high porosity values (large specific volumes) tend to promote compaction (negative dilatancy).

Some field observations are consistent with these results of critical state theory. For example, positive and negative dilatancies in deformation bands have been observed commonly where the porosity of the host rock is lower than 12% and higher than 18%, respectively (ANTONELLINI *et al.*, 1994).

The effect of the mean compressional normal stress is hard to evaluate from field data alone. However, some insights can be drawn from microstructural observations on sandstone samples after hydrostatic compaction experiments (ZHANG *et al.*, 1990; WONG and DAVID, 1992) demonstrating that the amount of grain crushing and compaction increases as does the pressure. These observations suggest that two generations of bands observed on limbs of a collapsed salt anticline (Fib. 1b) at Arches National Park may have developed under different stress states controlled by different thicknesses of the overburden during deformation. The older generation consists of bands with little or no cataclasis and the younger generation consists of bands with well-developed cataclasis. The first generation of bands may have formed during the growth of the salt anticline when the overburden was thin ($<100-200$ m), whereas the second generation may have developed during the collapse of the salt anticline when the overburden was thicker ($\sim 1000-2000$ m).

Positive dilatancy has been recognized at the tip of some of the deformation bands in low-porosity sandstones that show small amounts of cataclasis in their microstructure (ANTONELLINI *et al.*, 1994). It appears that, given a sufficiently tight grain packing and moderate mean compressive normal stresses, the micromechanics of deformation band growth is controlled by initial positive dilatancy as the grains roll and slide past each other. ANTONELLINI *et al.* (1994) have observed that the porosity increases as much as two-fold with respect to the host rock in patches (5–50 mm long) coplanar with the tip of deformation bands. This initial dilatancy may be a transient phenomenon that is followed by grain splitting at points of contact and porosity reduction as shearing progresses. This process, in combination with the stresses induced by frictional sliding, probably leads to grain crushing and rotation.

Discussion

Porosity Measurement Techniques

Two porosity profiles across the same deformation band but at different positions in the sample ($\sim$30 mm between the two profiles), one obtained via petrographic image analysis and the other via X-ray computerized tomography, are shown in Figure 7. The PIA porosity is 19% in the country rock and about 2% in the 1 mm-thick deformation band. The CT porosity (Fig. 7) ranges from 3 to 5% in the deformation band and from 16 to 22.5% in the host rock. It is apparent that image analysis allows one to resolve porosity in areas smaller than 1 mm^2, and therefore provides a very local measurement. On the other hand the porosity determined with CT is averaged within a volume (voxel) of 2 mm^3. This sampling volume has the same scale length as the width of the structures under examination. The CT porosity values (Fig. 7) are larger near and within the deformation band than the PIA porosity values, probably because of this relatively "large" sampling volume. Nonetheless, the CT porosity maps (Figs. 6a and b) provide an excellent representation of the spatial distribution of porosity and its small-scale variation in fault structures.

By calculating the average density of an image slice and by assuming that it is comprised solely of quartz, it is possible to calculate the average porosity of the slice. The average porosity of the slice in Figure 3b was calculated to be 16% using PIA methods and 17% using CT techniques. The PIA average porosity was calculated using porosity values obtained from a thin section cut at a distance of 30 mm from the plane of the CT scan, and using the geometric characteristics of the structures present in the CT scan. Considering that the average porosity includes the porosities of the host rock, the deformation bands and wall rock of the slip plane, we consider this to be quite a good match.

Conventional methods such as helium porosimetry (JOHNSON, 1983) are the most inexpensive on the market, but they measure the porosity of a core plug which is about 25 mm in diameter, therefore one cannot use them to determine the porosity of small structures (scale width of a few mm or less). Furthermore, helium porosimetry is unable to determine the skeleton porosity of sandstone nor any other spatial property of porosity that may be of interest in a microstructural study. The best use of helium porosimetry is when the rock contains an homogeneous porosity, at least at the scale of the size of the core plug, and when no secondary phases occupy the pore space (if the objective is to determine the skeleton porosity).

PIA techniques work very well where the sandstone is monomineralic, because of the definite contrast between the color of the grains and the epoxy. The epoxy impregnation has to be done with extreme care to allow a uniform penetration of the sample where the pore space is very narrow. Skeleton porosity can be measured with PIA, provided that the pore space is completely filled by the secondary phases, and these latter phases have a color that contrasts with that of the mineral grains.

When the automatic determination of the porosity is not satisfactory, it is always possible to manually point count the video image of the thin section which is faster and easier than point counting at the microscope. To speed up this procedure it is very convenient to superpose a grid on the video image. PIA techniques in combination with point counting are very well suited for porosity determinations, because the lower limit to the size of the structure on which they can be employed is controlled only by the resolution of the microscope and of the video image (sub-mm resolution). On the other hand, CT resolution is on the order of 1–2 mm. The disadvantage of PIA techniques is that they are two-dimensional; this is an unimportant limitation as long as the pore space is only slightly anisotropic.

Where PIA provides porosity measurements down to the sub-mm scale, CT is an excellent tool to produce maps of porosity variations in two and three dimensions. Porosity maps are very valuable to study how the porosity varies in proximity to a structure in a micro or mesoscale structural study. CT porosity is measured on a rock volume of a few mm^3, therefore, the porosity of structures at a scale smaller than 2–3 mm is averaged with the porosity of the surrounding material. This causes larger CT porosity values relative to PIA porosity values in the deformation band of Figure 7 and the difference between CT and point counting porosity in the wall rock of the slip plane (Fig. 5b). Other disadvantages of CT are its high cost and the inability to measure skeleton porosity.

Hydraulic Behavior of a Fault Zone

On the basis of the petrophysical properties and the structural characteristics of a fault zone in sandstone, one can predict that the low permeability cataclastic material of the deformation bands and of the wall rock of the slip planes may create a seal to the movement of the fluids in the direction perpendicular to the fault plane whereas the structural discontinuity of the slip plane may create a preferential pathway for fluid flow parallel to the fault. This result suggests an hydraulic model in which faults in sandstone are conduits along their length, but barriers across their thickness (Fig. 8). Such faults could compartmentalize the sandstone in which they develop or they may form hydrocarbon traps (DOWNEY, 1984; KNOTT, 1993). On the other hand, they could also act as conduits for hydrocarbons that move from the source rock into the reservoir rock or as "bypass" conduits (EDWARDS *et al.*, 1993) for fluids that move vertically across reservoirs separated by horizontal barriers.

The implications of this model are not only important to study the behavior of fluids in reservoirs and aquifers, but they also aid in constraining the effect of fluids on the dynamics of large-scale crustal faults. Fluids, in fact, are often reported to be associated with crustal fault zones (MCCAIG, 1989; KNIPE *et al.*, 1991; MOORE *et al.*, 1991; LOGAN, 1991). How fluids penetrate a fault zone is a matter of some

debate (RICE, 1992; BYERLEE, 1993). For example, SIBSON *et al.* (1975) propose that fluids are channeled along a fault zone as a result of dilatancy-induced pumping during seismic events. The lithologic characteristics of rocks next to a fault zone may also control the way fluids penetrate the zone. For example, in carbonate rocks fluids may penetrate a fault zone if extensive fracturing is localized in its proximity (KASTNING, 1977), whereas in sandstones the fluids may enter the fault zone because of the existence of a physical discontinuity between the rocks of the hanging wall and the rocks of the footwall (ANTONELLINI and AYDIN, 1994).

Once fluids have penetrated a fault zone, the existence of sealing structures could allow the maintenance of overpressures in the fault zone. These are essential elements for the fault models proposed by RICE (1992) and BYERLEE (1990, 1993). These models focus on the mechanical behavior of *weak* faults; i.e., faults where slip occurs despite the unfavorable orientation of the regional principal compressional stress direction (for example, the San Andreas Fault; ZOBACK *et al.*, 1987). One of the most plausible ways to produce a localized zone of weakness along such a fault is to create an area of elevated fluid pressure within the fault zone. In particular, according to BYERLEE (1993), the rupture of a sealed compartment may redistribute the overpressure to a larger volume and consequently trigger an earthquake. The existence of pressure seals in granite, next to faults simulated in laboratory experiments, has been reported by BLANPIED *et al.* (1992). In the context of this paper, the question is: do the cataclastic material and the diagenetic phenomena observed in fault zones in sandstone have the necessary sealing potential? Our study suggests that this is possible for the range of lithologies and physical conditions of these rocks. In fact, the cataclastic and recrystallized material in the wall rock of slip planes has very low permeability and porosity, so that it could form seals and/or create compartments in the fault zone.

Acknowledgments

This work has been funded by the Rock Fracture Project at Stanford University, and by a Phillips Petroleum Co. fellowship to M. Antonellini. Special thanks to R. Shupe, M. Queen and P. Lively at Conoco Inc. for the realization of the CT images presented in this work. Reviews of M. Blanpied, M. Cooke, D. Moore and an anonymous reviewer have greatly improved the manuscript.

REFERENCES

ANTONELLINI, M. A., AYDIN, A., and POLLARD, D. (1994), *Microstructure of Deformation Bands in Porous Sandstones at Arches National Park, Utah*, J. Struct. Geology *16*, 941–959.

ANTONELLINI, M. A., and AYDIN, A. (1994), *Effect of Faulting on Fluid Flow in Porous Sandstones: Petrophysical Properties*, The Am. Assoc. of Petroleum Geologists Bull. *78*, 355–377.

ANTONELLINI, M. A., and AYDIN, A., *Effect of Faulting on Fluid Flow in Porous Sandstones: Geometric Properties*, submitted to The Am. Assoc. of Petroleum Geologists Bull.

AYDIN, A. (1978), *Small Faults Formed as Deformation Bands in Sandstone*, Pure and Appl. Geophys. *116*, 913–930.

AYDIN, A., and JOHNSON, A. M. (1983), *Analysis of Faulting in Porous Sandstones*, J. Struct. Geology *5*, 19–31.

BLANPIED, M. L., LOCKNER, D. A., and BYERLEE, J. D. (1992), *An Earthquake Mechanism Based on Rapid Sealing of Faults*, Nature *358*, 574–576.

BOURBIÈ, T., COUSSY, O., and ZINSZNER, B., *Acoustics of Porous Media* (Gulf Publishing Company, Technip, Paris 1987).

BROOKS, R. A., and DICHIRO, G. (1976), *Principles of Computer-assisted Tomography in Radiographic and Radioisotopic Imaging*, Phys. Med. Biol. *21*, 689–732.

BYERLEE, J. (1990), *Friction, Overpressure and Fault Normal Compression*, Geophys. Res. Lett. *17*, 2109–2112.

BYERLEE, J. (1993), *Model for Episodic Flow of High-pressure Water in Fault Zones before Earthquakes*, Geology *21*, 303–306.

DOWNEY, M. W. (1984), *Evaluating Seals for Hydrocarbon Accumulations*, The Am. Assoc. of Petroleum Geologists Bull. *68*, 1752–1763.

EHRLICH, R., CRABTREE, S. J., HORKOWITZ, K. O., and HORKOWITZ, J. P. (1991), *Petrography and Reservoir Physics: I, II and III*, The Am. Assoc. of Petroleum Geologists Bull. *75*, 1547–1562.

EDWARDS, H. E., BECKER, A. D., and HOWELL, J. A., *Compartmentalization of an Aeolian sandstone by structural heterogeneities: Permo-Triassic Hopeman Sandstone, Moray Firth, Scotland.* In *Characterization of Fluvial and Aeolian Reservoirs* (eds. North, C. P., and Prosser, D. J.) (Geological Society Special Publication, No. 73 1993) pp. 339–365.

HARDMANN, R. F. P., and BOOTH, J. E., *The significance of normal faults in the exploration and production of North Sea hydrocarbons.* In *The Geometry of Normal Faults* (eds. Roberts A. M., Yielding, G., and Freeman, B.) (Geological Society Special Publication, No. 56 1991) pp. 1–13.

HENDERSON, L. H. (1939), *Detailed Geological Mapping and Fault Studies of the San Jacinto Tunnel Line and Vicinity*, J. Geology *47*, 314–324.

HOUNSFIELD, G. N., *A Method of and Apparatus for Examination of a Body by Radiation such as X- or Gamma Radiation* (British Patent no. 1283915 1972).

JOHNSON, G. R., *Rock property measurements and analysis of selected igneous, sedimentary, and metamorphic rocks from worldwide localities* (U.S. Geological Survey Open-file Report 83–0736, Denver 1983).

KASTNING, E. H., *Faults as positive and negative influences on ground-water flow and conduit enlargement.* In *Hydrologic-Problems in Karst Regions* (eds. Dilamarter, R. R., and S. C. Csallany) (Western Kentucky University, Bowling Green 1977) pp. 193–201.

KNIPE, R. J., AGAR, S. M., and PRIOR, D. J. (1991), *The Microstructural Evolution of Fluid Flow Paths in Semi-lithified Sediments from Subduction Complexes*, Philosophical Trans. Roy. Soc. London A *335*, 261–273.

KNOTT, S. D. (1993), *Fault Seal Analysis in the North Sea*, The Am. Assoc. Petroleum Geologists Bull. *77*, 778–792.

LOGAN, J. M. (1991), *The Influence of Fault Zones on Crustal-scale Fluid Transport*, The Am. Assoc. Petroleum Geologists Bull. *75*, 623.

MACLAY, R. W., and LAND, L. F. (1988), *Simulation of Flow in the Edwards Aquifer, San Antonio Region, Texas, and Refinement of Storage and Flow Concepts*, U.S. Geological Survey Water-Supply Paper, *2336*, A1–A48.

MCCAIG, A. M. (1989), *Fluid Flow through Fault Zones*, Nature *340*, 600.

MOORE, J. C., BROWN, K. M., HORATH, F., COCHRANE, G., MACKAY, M., and MOORE, G. (1991), *Plumbing Accretionary Prisms: Effects of Permeability Variations*, Philosophical Trans. Roy. Soc. London A *335*, 275–288.

NELSON, R. A., *Geologic Analysis of Naturally Fractured Reservoirs* (Gulf Publishing Company, Houston, Texas 1985).

PARRY, R. H. G. (1960), *Triaxial Compression and Extension Tests on Remoulded Saturated Clay*, Geotechnique *10*, 166–180.

PITTMAN, E. D. (1981), *Effect of Fault-related Granulation on Porosity and Permeability of Quartz Sandstones, Simpson Group (Ordovician), Oklahoma*, The Am. Assoc. Petroleum Geologists Bull. *65*, 2381–2387.

RICE, J. R., *Fault stress states, pore pressure distributions, and the weakness of the San Andreas Fault*. In *Earthquake Mechanics and Transport Properties of Rocks* (eds. Evans, B., and Wong, T. F.) (Academic Press, London 1992) pp. 475–503.

ROBISON, J. H., STEPHENS, D. M., LUCKEY, R. R., and BALDWIN, D. A., *Water Levels in Periodically Measured Wells in the Yucca Mountain Area, Nye County, Nevada, 1981–1987* (U.S. Geological Survey Open-file Report 88–0468, Denver 1988).

SCHOFIELD, A. N., and WROTH, P., *Critical State Soil Mechanics* (McGraw Hill, New York 1968).

SIBSON, R. H., MOORE, J. McM., and RANKIN, A. H. (1975), *Seismic Pumping—a Hydrothermal Fluid Transport Mechanism*, J. Geological Soc. London *131*, 653–659.

SLEEP, N. H., and BLANPIED, M. L. (1992), *Creep Compaction and the Weak Rheology of Major Faults*, Nature *359*, 687–692.

UNDERHILL, J. R., and WOODCOCK, N. H. (1987), *Faulting mechanisms in high-porosity sandstones; New Red Sandstone, Arran, Scotland*. In *Deformation of Sediments and Sedimentary Rocks* (eds. Jones, M. E., and Preston, R. M. F.) (Special Publication of the Geological Society of London, *29* 1987) pp. 91–105.

VINEGAR, H. J., DE WAAL, J. A., and WELLINGTON, S. L. (1991), *CT Studies of Brittle Failure in Castlegate Sandstone*, Int. J. Rock Mech. Min. Sci. and Geomech. Abstr. *28*, 441–448.

WELLINGTON, S. L., and VINEGAR, H. J. (1987), *X-ray Computerized Tomography*, J. Petroleum Tech. *87*, 885–898.

WONG, T. F., and DAVID, C. (1992), *Grain Crushing and Pore Collapse as Controlling Mechanisms for the Brittle-Ductile Transition*, EOS *73*, 515.

WOOD, D. M., *Soil Behavior and Critical State Soil Mechanics* (Cambridge University Press, England 1990).

ZHANG, J., WONG, T. F., and DAVIS, D. M. (1990), *Micromechanics of Pressure-induced Grain Crushing in Porous Rocks*, J. Geophys. Res. *95*, 341–352.

ZOBACK, M. D., ZOBACK, M. L., MOUNT, VAN S., SUPPE, J., EATON, J. P., HEALY, J. H., OPPENHEIMER, D. H., REASENBERG, P. A., JONES, L. M., RALEIGH, C. B., WONG, I. G., SCOTTI, O., and WENTWORTH, C. M. (1987), *New Evidence on the State of Stress of the San Andreas Fault System*, Science *238*, 1105–1111.

(Received October 6, 1993, revised/accepted March 16, 1994)